CHEMISTRY
A European Journal

Supporting Information

A Pseudo-Octahedral Cobalt(II) Complex with Bispyrazolylpyridine Ligands Acting as a Zero-Field Single-Molecule Magnet with Easy Axis Anisotropy

Luca Rigamonti,*[a] Nathalie Bridonneau,[a, e] Giordano Poneti,[b, f] Lorenzo Tesi,[b] Lorenzo Sorace,[b] Dawid Pinkowicz,[c] Jesus Jover,[d] Eliseo Ruiz,[d] Roberta Sessoli,[b] and Andrea Cornia[a]

chem_201801026_sm_miscellaneous_information.pdf

Author Contributions

L.R. conceived and designed the experiments; L.R. and N.B. performed the synthesis and crystallization; G.P. performed the dc and ac magnetic measurements; L.T. performed the CTM and dc magnetic measurements and helped L.S. with the single-crystal EPR experiments; L.S. performed the EPR experiments and simulations and wrote the code for the analysis of the CTM measurements by using the Griffith Hamiltonian; D.P. performed the single-crystal X-ray diffraction studies; J.J. and E.R. performed the theoretical calculations; all authors analyzed the data; R.S. and A.C. contributed reagents, materials, and analytical tools; L.R. wrote the paper with the help of all the coauthors.

Supporting Information (SI)

Index

Experimental Section

X-ray crystal structure determination

Single-crystal X-ray diffraction studies were carried out with a Bruker D8 Quest Eco Photon50 CMOS diffractometer equipped with a Mo-Kα generator (graphite monochromator, λ = 0.71073 Å) at 295(2) and 161(2) K for **1** and 120(2) K for **2** (see Table S1 for full details). Data reduction and cell refinements were performed using SAINT.[S1] Intensities of reflections were corrected for the sample absorption using multi-scan methods (SADABS).[S2] The structure was solved using direct methods and refined anisotropically using weighted full-matrix least-squares on F^2 with the SHELXL-2014/7 program.[S3] Structure solution resolved the positions of the metals and most of the Cl, O, N and C atoms. The remaining non-hydrogen atoms were located by alternating cycles of least-squares refinements and difference Fourier maps. Hydrogen atoms were placed at calculated positions and refined as riding with U_{iso}(H) fixed at 1.2 U_{eq}(C). The program Mercury 3.9[S4] was used for graphics. CCDC 1812294, 1812295 and 1812293 contain the supplementary crystallographic data for **1** at 161 and 295 K and **2** at 120 K, respectively. These data can be obtained free of charge from The Cambridge Crystallographic Data Centre via www.ccdc.cam.ac.uk/data_request/cif. Room temperature unit cell parameters for **1**, **2** and **3** were also collected (Table S2) with a four-circle Bruker X8-APEX diffractometer equipped with a Mo-Kα generator (λ = 0.71073 Å) and an area detector controlled by Bruker-Nonius X8APEX software.

Magnetic measurements

Direct current (dc) measurements at ambient pressure were carried out using a Quantum Design Magnetic Property Measurement System (MPMS) equipped with a Superconducting Quantum Interference Device (SQUID) magnetometer and a 5 T magnet on a 19.27 mg grinded polycrystalline sample of **1** pelletized in a Teflon® matrix. The temperature dependence of the magnetization (M) was followed from 2 to 300 K by applying a 10 kOe field (H_{DC}) from 300 to 30 K and a 1 kOe field below 30 K to reduce magnetic saturation effects. Molar magnetic susceptibility (χ_M) was then evaluated as $\chi_M = M_M/H$. The field dependence of isothermal magnetization, M_M, at 7.0, 5.0, 3.0 and 1.8 K was measured in applied fields up to 50 kOe. The response was corrected by the diamagnetic contributions of sample holder, Teflon® and compound diamagnetism, estimated as –360.96 10^{-6} emu mol^{-1} from Pascal constants.[S5] Alternating current (ac) data were collected using a Quantum Design Physical Property Measurement System (PPMS) susceptometer in the 10–10000 Hz range on 8.66 and 35.28 mg grinded polycrystalline samples of **1**

and **3**, respectively, pelletized in a Teflon® matrix. Additional in-field ac data on **3** were also recorded with the Quantum Design MPMS SQUID magnetometer in the 10–1000 Hz range. The ac susceptibility data were analysed within the extended Debye model[S6] in which a maximum in the out-of-phase component χ_M'' of the complex susceptibility is observed when the relaxation time τ equals $(2\pi\nu)^{-1}$. The frequency dependence of χ_M'' of the investigated samples at constant T was fitted using the equation:

$$\chi_M''(\omega) = (\chi_T - \chi_S)[(\omega\tau)^{1-\alpha}\cos(\alpha\pi/2)]/[1 + 2(\omega\tau)^{1-\alpha}\sin(\alpha\pi/2) + (\omega\tau)^{2-2\alpha}] \quad \text{(S1)}$$

where $\omega = 2\pi\nu$, χ_T and χ_S are the isothermal and adiabatic susceptibilities, *i.e.*, the susceptibilities observed in the two limiting cases $\nu \rightarrow 0$ and ∞, respectively, and α is a parameter that accounts for a distribution of relaxation times.

Cantilever Torque Magnetometry (CTM) measurements

A single crystal of **1** of volume about $0.5 \times 0.5 \times 0.5$ mm^3 was placed on a square acetate foil (sides ca. 3×3 mm) with Apiezon vacuum grease and its faces were indexed with an SCD Oxford Xcalibur3 X-Ray diffractometer using a Cu source (Cu-Kα = 1.54060 Å). The crystal on the acetate foil was then placed on a home made two-legged CuBe cantilever, separated by 0.1 mm from a gold plate. This was inserted into an Oxford Instruments MAGLAB2000 platform with automated rotation of the cantilever chip and a 12 T vertical magnet. The measurements were performed rotating the cantilever and recording the capacitance with an Andeen-Hegerling 2500 A Ultra Precision Capacitance Bridge. For constructive reasons the rotation angle could only range from 0 to 200°, which however already provides redundant angular data due to the 180° periodicity expected for any anisotropic paramagnetic system. At each temperature (T = 10, 30, 50, 80, 100 and 150 K) the rotation was performed also in zero field in order to correct data for the deflection due to the mass of both sample and cantilever. The torquemeter was always operated in the linear response regime and an overall scale factor (dependent on the model applied, i.e. spin Hamiltonian, Griffith Hamiltonian or MOLCAS-calculated torque data) was refined to account for the sample mass (about 80 μg), which was impossible to measure with due accuracy.

Electron paramagnetic resonance (EPR) measurements

Continuous Wave (CW) X-band ($\nu \sim 9.4$ GHz) EPR spectra of all samples were recorded on a Bruker Elexsys E500 spectrometer equipped with a SHQ cavity. Low-temperature measurements were obtained using an Oxford Instruments ESR900 continuous flow helium cryostat. The angular dependence of single-crystal spectra has been measured in steps of 5° by using a digital programmable goniometer (ER218PG1, Bruker BioSpin).

***Ab initio* calculations**

The calculations of the second-order magnetic anisotropy (or zero field splitting, *zfs*) parameters (*D* and *E*) was carried out with two different software packages, MOLCAS[S7] and Orca,[S8] using the experimental geometries as found in the X-ray investigations. We employed MOLCAS (along with the SINGLE_ANISO[S9,S10] code) to carry out a CASSCF/CASPT2 calculation of the energy states of **1**. After that, the spin-orbit coupling was introduced, as implemented in the SO-RASSI approach, to mix up these energies and obtaining the final energy states. In these calculations we employed an all electron ANO-RCC basis set with two different contractions:[S11–S14] *i*) standard, Co (6*s*5*p*4*d*2*f*), N (4*s*3*p*2*d*1*f*, 3*s*2*p* for atoms not attached to Co), O (3*s*2*p*), C (3*s*2*p*) and H (2*s*), *ii*) larger, Co (7*s*6*p*4*d*3*f*2*g*), N (5*s*4*p*3*d*2*f*, 3*s*2*p*1*d* for N atoms not attached to Co), O (4*s*3*p*1*d*), C (3*s*2*p*) and H (2*s*). Both basis sets were applied only to the molecular structure of **1** at 161 K in order to test the dependency of the calculated *D* and *E* values from the basis set, while standard one was used to evaluate both structures at 161 and 295 K. In order to improve the convergence of the CASPT2 calculation, the orbitals with small population in the active site (less than 0.1 of the density) were kept frozen.

The CASSCF/NEVPT2[S15–S17] procedure was employed in the calculations with Orca. In this case all the atoms are described by the standard def2-TZVPP and larger def2-QZVPP basis sets,[S18,S19] including the corresponding auxiliary basis sets for correlation and Coulomb fitting. In both sets of calculations, the active space is formed by the seven *d* electrons of the cobalt(II) centre and the 5*d* orbitals (7,5), and all the quadruplet (10) and doublet (40) states were taken into account.

The energy order of the 3*d* orbitals for **1** was computed with Orca in the CASSCF calculation, employing the *Ab Initio Ligand Field* method (AILF) to derive the *d*-orbital energy splitting using the experimental X-ray structure at 161 K.

Torque values at different temperatures and applied fields for rotations around the different axes were also computed from the magnetization values extracted from MOLCAS/CASSCF calculation and application of eq 2 in the main text. The magnetization vector was calculated at 18 rotation angles every 10°, corresponding to a global rotation of 180°.

Table S1. Crystallographic data and refinement parameters for **1** (Co) and **2** (Zn) collected with the Bruker D8 Quest Eco Photon50 CMOS diffractometer.

	1 (T = 295 K)	**1** (T = 161 K)	**2** (T = 120 K)
formula	$C_{26}H_{22}Cl_2CoN_{10}O_{12}$	$C_{26}H_{22}Cl_2CoN_{10}O_{12}$	$C_{26}H_{22}Cl_2N_{10}O_{12}Zn$
formula weight	796.36	796.36	802.83
crystal system	monoclinic	monoclinic	monoclinic
space group	*C*2/*c* (n. 15)	*C*2/*c* (n. 15)	*C*2/*c* (n. 15)
crystal description	yellow-orange plate	yellow-orange plate	colourless plate
crystal size [mm^3]	0.30 × 0.16 × 0.12	0.20 × 0.16 × 0.04	0.21 × 0.15 × 0.05
a [Å]	23.5908(9)	23.5857(14)	23.6567(7)
b [Å]	10.5891(4)	10.3842(6)	10.1802(3)
c [Å]	15.9727(6)	15.9185(10)	16.0292(4)
β [°]	127.5430(10)	127.542(2)	127.522(1)
V [Å^3], Z	3163.7(2), 4	3091.2(3), 4	3061.7(2), 4
ρ_{calcd} [g cm^{-3}]	1.672	1.711	1.742
μ [mm^{-1}]	0.792	0.811	1.060
T [K]	295(2)	161(2)	120(2)
$2\theta_{max}$ [°]	51.44	49.48	52.75
collected/indep reflns	15425/3009	17031/2647	17240/3123
R_{int}	0.0345	0.0396	0.0408
restraints/parameters	0/231	0/231	0/232
R_1, wR_2 ($I > 2\sigma(I)$)	0.0455, 0.1205	0.0381, 0.0902	0.0290, 0.0677
R_1, wR_2 (all data)	0.0544, 0.1262	0.0442, 0.0933	0.0378, 0.0713
goodness-of-fit on F^2	1.059	1.049	1.023
max./min. residual density [e A^{-3}]	0.768, –0.578	0.746, –0.584	0.372, –0.519
completeness	0.998	0.995	0.998

Table S2. Room temperature unit cell parameters for **1**, **2** and **3** collected with the four-circle Bruker X8-APEX diffractometer.

	1 (Co)	**2** (Zn)	**3** ($Co_{0.05}Zn_{0.95}$)
formula	$C_{26}H_{22}Cl_2CoN_{10}O_{12}$	$C_{26}H_{22}Cl_2N_{10}O_{12}Zn$	$C_{26}H_{22}Cl_2Co_{0.05}N_{10}O_{12}Zn_{0.95}$
formula weight	796.36	802.83	802.51
crystal system	monoclinic *C*	monoclinic *C*	monoclinic *C*
T [K]	298(2)	298(2)	298(2)
a [Å]	23.58(3)	23.66(2)	23.60(3)
b [Å]	10.57(1)	10.577(9)	10.561(9)
c [Å]	15.97(2)	16.01(2)	15.99(2)
β [°]	127.66(3)	127.66(2)	127.52(2)
V [Å^3]	3151(2)	3171(6)	3161(4)
Fitted/total reflns	395/408	219/248	358/365

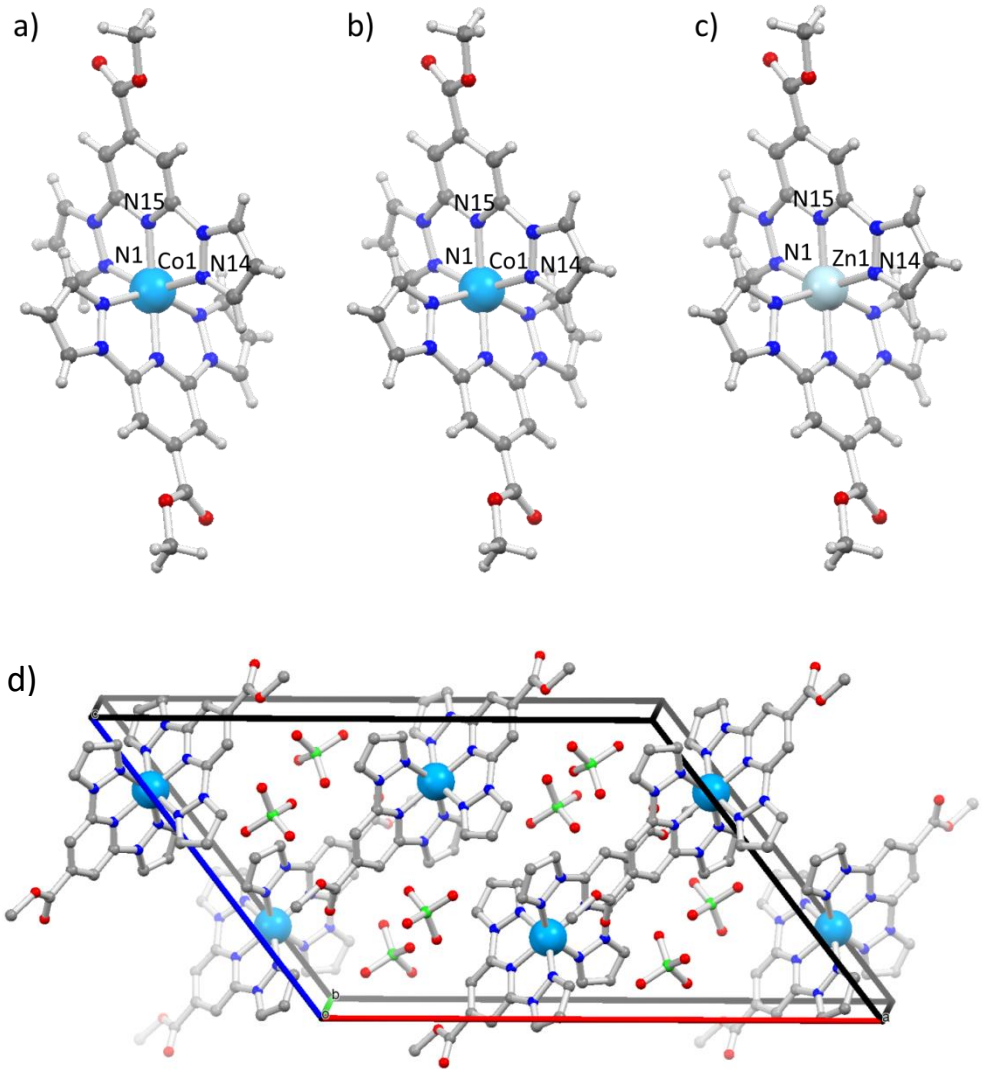

Figure S1. View of the $[M(bpp\text{-}COOMe)_2]^{2+}$ cation along *b* in a) **1** at 161 K, b) **1** at 295 K and c) **2** at 120 K; d) Crystal packing of **1** at low *T* with the perchlorate positions as representative for all the structures (colour code: Zn = light blue, Co = azure, Cl = green, O = red, N = blue, C = grey, H = white or omitted for clarity in the crystal packing).

Table S3. Hydrogen bonds in **1** at 295 K (Å and °).

D–H···A[a,b]	***d*(H···A)**	***d*(D···A)**	**<(DHA)**
C1–H1···O17#1	2.46	3.291(4)	148.9
C3–H3···O2#2	2.41	3.321(5)	165.7
C6–H6···O2#2	2.55	3.456(5)	165.0
C8–H8···O4#3	2.52	3.367(6)	151.8
C11–H11···O4#3	2.34	3.234(6)	160.0
C13–H13···O1#4	2.47	3.360(7)	159.8

[a] *d*(D–H) are fixed to 0.93 Å; [b] symmetry transformations used to generate equivalent atoms: #1 = x+1/2,–y+1/2,z–1/2; #2 = –x+1/2,–y+1/2,–z; #3 = –x+1/2,y+1/2,–z+1/2; #4 = –x,–y,–z

Table S4. Hydrogen bonds in **1** at 161 K (Å and °).

D–H···A[a,b]	***d*(H···A)**	***d*(D···A)**	**<(DHA)**
C1–H1···O17#1	2.46	3.252(3)	147.5
C3–H3···O2#2	2.33	3.261(4)	165.3
C6–H6···O2#2	2.50	3.420(4)	164.1
C8–H8···O4#3	2.46	3.291(4)	146.1
C11–H11···O4#3	2.40	3.284(4)	155.2
C13–H13···O1#4	2.47	3.360(7)	159.8

[a] *d*(D–H) are fixed to 0.93 Å; [b] symmetry transformations used to generate equivalent atoms: #1 = x+1/2,–y+1/2,z–1/2; #2 = –x+1/2,–y+1/2,–z; #3 = –x+1/2,y+1/2,–z+1/2; #4 = –x,–y,–z

Table S5. Hydrogen bonds in **2** at 120 K (Å and °).

D–H···A[a,b]	***d*(H···A)**	***d*(D···A)**	**<(DHA)**
C1–H1···O17#1	2.42	3.249(2)	145.2
C3–H3···O2#2	2.28	3.208(3)	165.6
C6–H6···O2#2	2.48	3.403(3)	163.2
C8–H8···O4#3	2.48	3.304(3)	145.1
C11–H11···O4#3	2.44	3.336(3)	156.3
C13–H13···O1#4	2.51	3.421(3)	160.8

[a] *d*(D–H) are fixed to 0.93 Å; [b] symmetry transformations used to generate equivalent atoms: #1 = x+1/2,–y+1/2,z–1/2; #2 = –x+1/2,–y+1/2,–z; #3 = –x+1/2,y+1/2,–z+1/2; #4 = –x,–y,–z

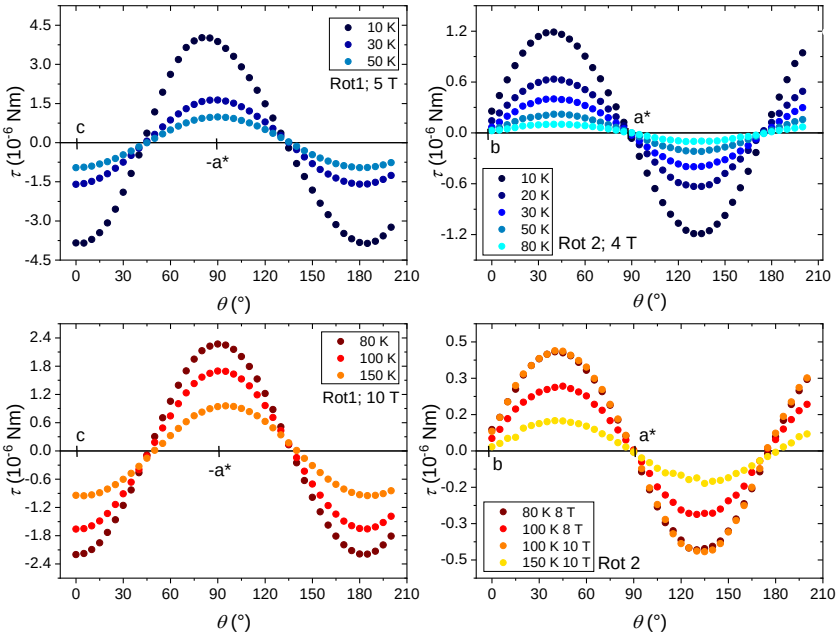

Figure S2. Experimental data obtained by CTM for the two rotations, Rot1 and Rot2, of **1** at several temperatures and for different applied magnetic fields.

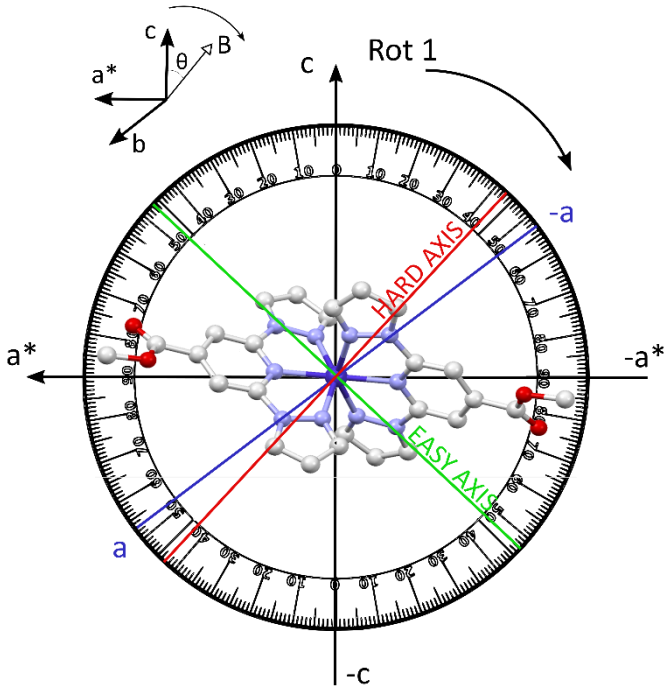

Figure S3. Sketch of the information provided by CTM in Rot1 when scanning the magnetic field in the *a***c* plane. The orientation of the magnetic field is defined by the angle θ which is measured clockwise from the *c* axis (at $\theta = 0°$ the magnetic field is parallel to *c*, whereas at $\theta = 90°$ it is parallel to –*a**).

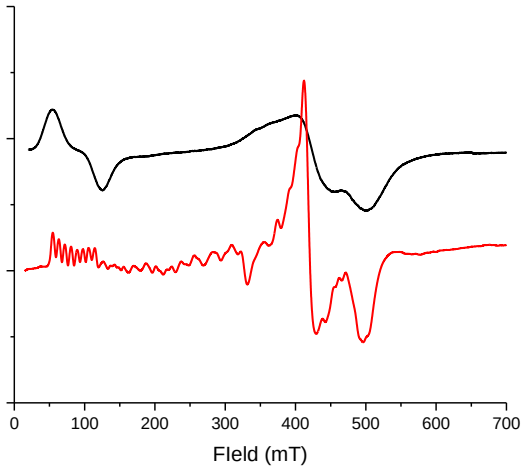

Figure S4. Comparison of experimental X-band powder EPR spectra of **1** (black trace) and **3** (red trace), measured at 10 K.

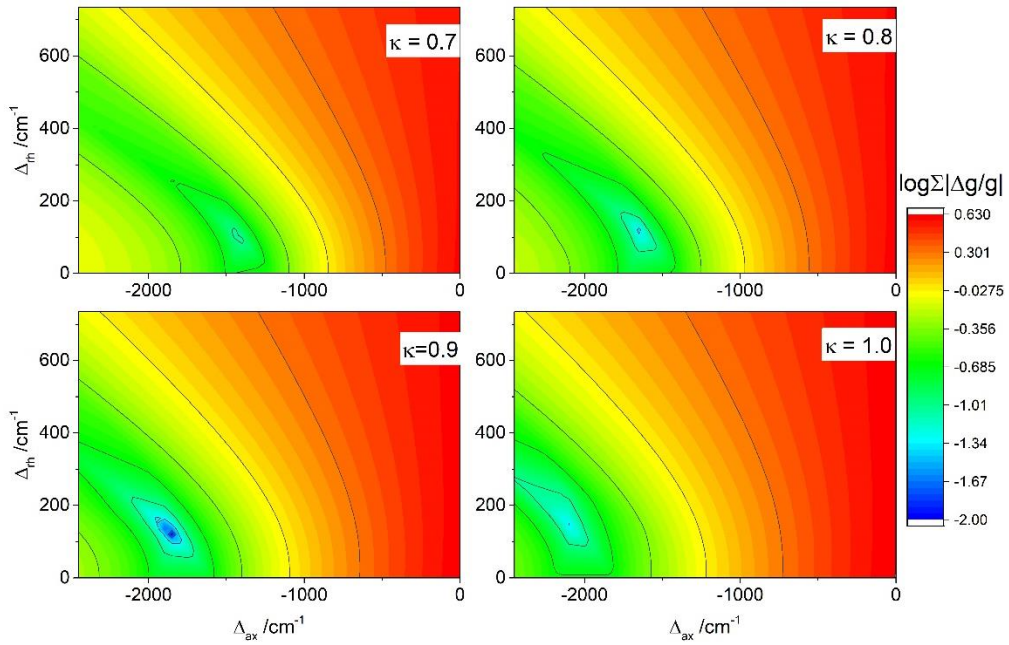

Figure S5. Dependence of the relative difference between experimental and calculated g_{eff} values (using Griffith model) on $\Delta_{\text{ax}}/\Delta_{\text{rh}}$ for different κ values, assuming $\lambda = -180$ cm^{-1}. The difference is reported as $\log\left(\sum_{i=1,2,3}\left(\frac{\left|g^{eff}_{i,\text{exp}} - g^{eff}_{i,cal}\right|}{g^{eff}_{i,\text{exp}}}\right)\right)$.

Table S6. Energy differences (cm^{-1}) between ground doublet and excited KDs calculated with spin Hamiltonian reproducing magnetic data and with Griffith Hamiltonian reproducing EPR spectrum (see text for more details).

Model	**1st exc.**	**2nd exc.**	**3rd exc.**	**4th exc.**	**5th exc.**
Spin Hamiltonian	127	–			
Griffith Hamiltonian	210	558	819	2334	2380

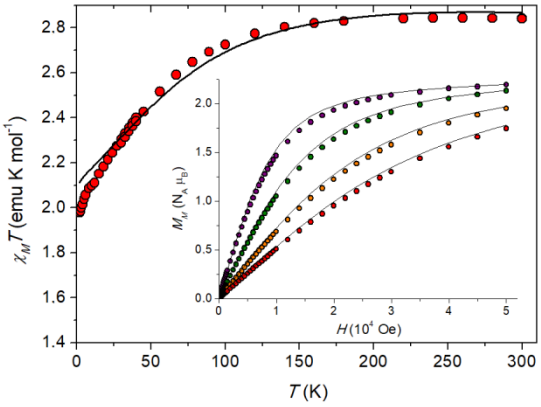

Figure S6. Simulation (black lines) of dc magnetic data (dots) of **1** obtained using Griffith Hamiltonian with parameters reproducing the g_{eff} values determined by EPR.

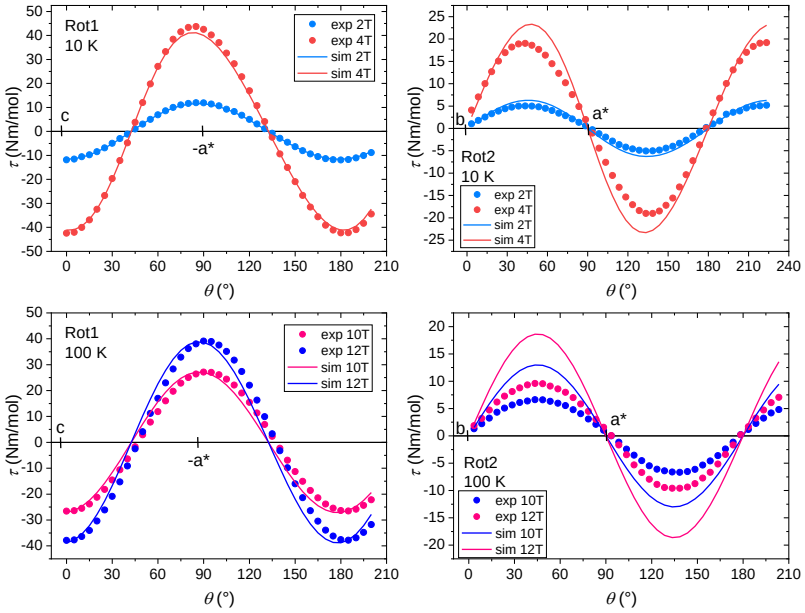

Figure S7. Simulation (lines, N m mol^{-1}), as implemented by a home-written MATLAB code exploiting EasySpin functions,[S20] of representative CTM data (dots) of **1** obtained using Griffith Hamiltonian with parameters reproducing the g_{eff} values determined by EPR.

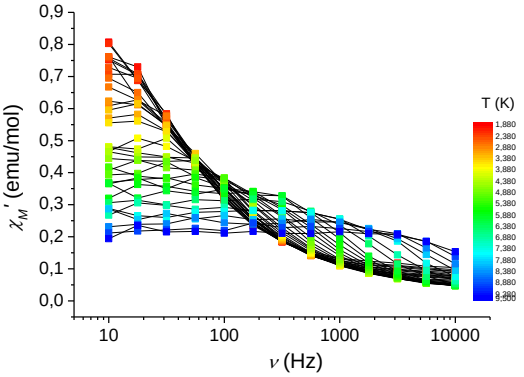

Figure S8. Real component of the ac susceptibility, χ_M', of **1** measured at 1 kOe applied static field in the 10–10000 Hz frequency range and in the 1.9(red)–9.5(blue) K temperature range; grey lines are a guide for the eye.

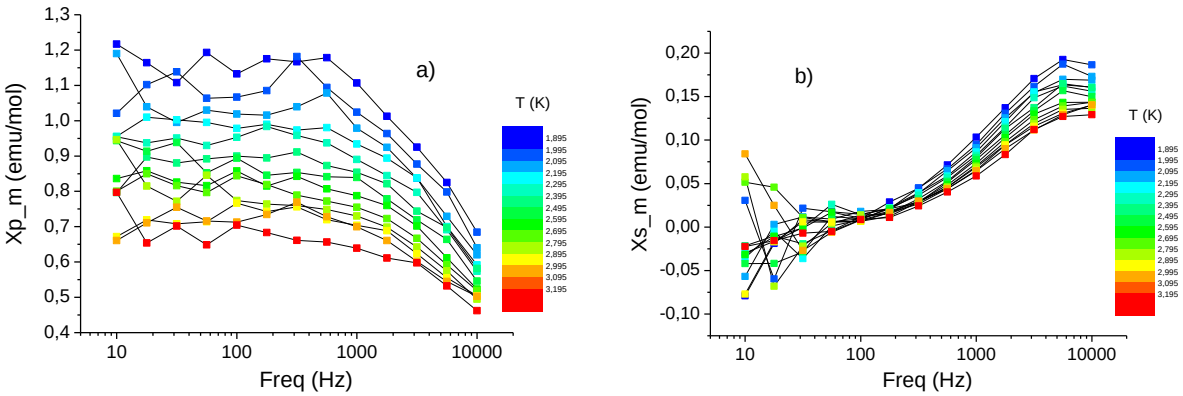

Figure S9. a) Real (χ_M') and b) imaginary (χ_M'') component of the ac susceptibility of **3** measured in zero applied static field in the 10–10000 Hz frequency range and in the 1.9(blue)–3.2(red) K temperature range; grey lines are a guide for the eye.

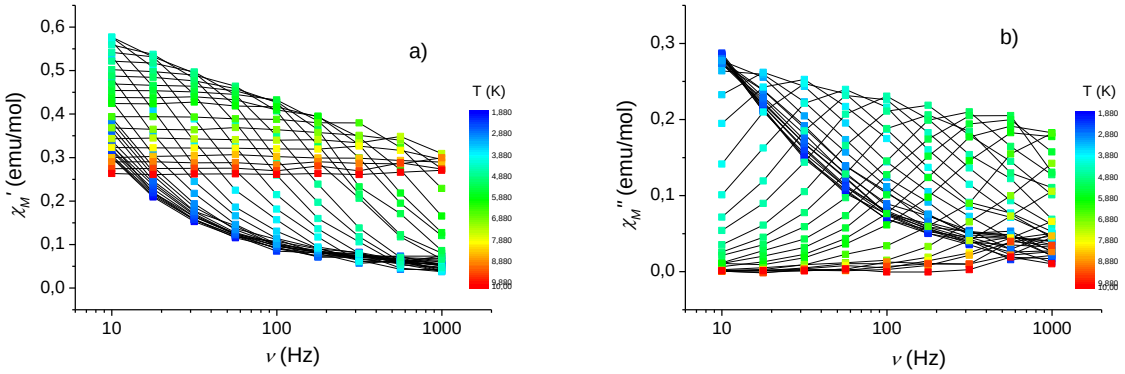

Figure S10. a) Real (χ_M') and b) imaginary (χ_M'') component of the ac susceptibility of **3** measured in 1 kOe applied static field in the 10–1000 Hz frequency range and in the 1.9(blue)–10.0(red) K temperature range; grey lines are a guide for the eye.

Table S7. ORCA/CASSCF computed spin-free (δ_E) and spin-orbit (Δ_E) state energies (cm^{-1}) for **1**.

Spin-free states (δ_E) and spin		Spin-orbit states (Δ_E)
0.0	3/2	0.0 196.1
364.7	3/2	653.5 943.7
1754.6	3/2	2056.5 2157.4
6915.2	3/2	7223.8 7270.9
7203.4	3/2	7538.8 7603.9
7773.9	3/2	8097.1 8193.1
14441.4	1/2	14766.0
14719.2	3/2	15102.0 15110.3
15426.6	1/2	15754.8
19868.5	1/2	20074.3
20109.6	1/2	20336.2
20143.2	1/2	20588.6
20693.2	1/2	21073.3

Table S8. ORCA/NEVPT2 computed spin-free (δ_E) and spin-orbit (Δ_E) state energies (cm^{-1}) for **1**.

Spin-free states (δ_E) and spin		Spin-orbit states (Δ_E)
0.0	3/2	0.0 179.4
467.4	3/2	722.0 981.9
2165.3	3/2	2427.2 2518.8
9223.8	3/2	9485.0 9518.0
9597.1	3/2	9872.6 9922.6
10048.7	1/2	10368.4
10347.6	3/2	10614.6 10722.6
11369.4	1/2	11693.0
18183.3	1/2	18373.9
18547.2	1/2	18718.0
18561.3	1/2	18957.1
19141.9	3/2	19359.8 19497.5
19371.2	1/2	19787.1

Table S9. MOLCAS/CASSCF computed spin-free (δ_E) and spin-orbit (Δ_E) state energies (cm^{-1}) for **1**.

Spin-free states (δ_E) and spin		Spin-orbit states (Δ_E)
0.0	3/2	0.0 195.1
368.9	3/2	655.0 944.4
1751.7	3/2	2053.9 2154.2
7032.8	3/2	7339.0 7385.4
7322.1	3/2	7655.1 7720.8
7883.8	3/2	8205.6 8300.7
14507.7	1/2	14832.0
14971.8	1/2	15351.4
15453.9	1/2	15358.6
19995.3	1/2	15781.5
20219.6	1/2	20195.9
20259.5	1/2	20451.4
20809.7	3/2	20702.4 21184.8

Table S10. MOLCAS/CASPT2 computed spin-free (δ_E) and spin-orbit state (Δ_E) energies (cm^{-1}) for **1**.

Spin-free states (δ_E) and spin		Spin-orbit states (Δ_E)
0.0	3/2	0.0 191.0
364.6	3/2	648.2 928.8
1842.7	3/2	2134.3 2231.3
7283.5	3/2	7579.1 7623.2
7539.9	3/2	7870.2 7941.6
8814.3	3/2	9115.0 9198.3
12757.6	1/2	13075.5
13810.1	1/2	14132.3
16408.7	1/2	16756.7
18050.3	1/2	16764.3
18707.8	1/2	18398.5
18739.6	1/2	18830.8
19102.0	3/2	19145.9 19513.8

Table S11. *D*, *E*, diagonalized $\bar{\boldsymbol{g}}$ and $\bar{\boldsymbol{D}}$ matrices and energy difference between the ground and the first excited KD (Δ_E) computed using the structure of **1** at 295 K with different methods and the standard basis set (see Experimental Section above). For comparison, the first excitation energy (δ_E) in the absence of SOC for the ground state is also reported.

Method	g_{xx}, g_{yy}, g_{zz}	D_{xx}, D_{yy}, D_{zz} (cm^{-1})	D (cm^{-1})	E (cm^{-1})	Δ_E (cm^{-1})	δ_E (cm^{-1})
ORCA/CASSCF	2.138, 1.937, 3.081	48.54, 14.63, –63.17	–94.8	17.0	198.4	352.5
ORCA/NEVPT2	2.134, 1.956, 3.010	42.49, 15.63, –58.12	–87.2	13.4	180.5	463.1
MOLCAS/CASSCF	2.153, 1.958, 3.084	49.11, 13.53, –62.64	–94.0	17.8	197.8	359.4
MOLCAS/CASPT2	2.137, 1.958, 3.068	47.02, 14.35, –61.37	–92.1	16.3	192.6	360.6

Table S12. *D*, *E*, diagonalized $\bar{\boldsymbol{g}}$ and $\bar{\boldsymbol{D}}$ matrices and energy difference between the ground and the first excited KD (Δ_E) computed using the structure of **1** at 161 K with different methods and the larger basis set (see Experimental Section above). For comparison, the first excitation energy (δ_E) in the absence of SOC for the ground state is also reported.

Method	g_{xx}, g_{yy}, g_{zz}	D_{xx}, D_{yy}, D_{zz} (cm^{-1})	D (cm^{-1})	E (cm^{-1})	Δ_E (cm^{-1})	δ_E (cm^{-1})
ORCA/CASSCF	2.159, 1.944, 3.071	49.61, 13.15, –62.77	–94.2	18.2	198.6	363.4
ORCA/NEVPT2	2.157, 1.961, 3.004	43.84, 14.04, –57.88	–86.8	14.9	181.1	469.0
MOLCAS/CASSCF	2.159, 1.957, 3.081	49.90, 12.60, –62.50	–93.8	18.7	198.3	354.9
MOLCAS/CASPT2	2.242, 1.957, 3.049	55.43, 5.94, –61.37	–92.1	24.7	203.1	382.5

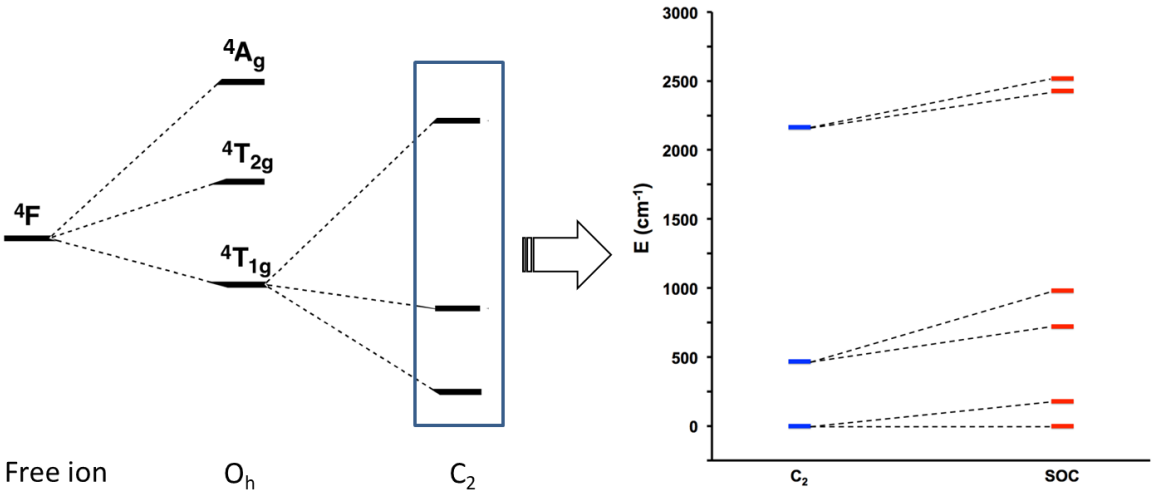

Figure S11. Effect of distortion of the octahedral coordination geometry and spin-orbit coupling on the energy levels of **1**. The energy splitting given in the right panel is scaled with respect to the energy levels computed by ORCA/NEVPT2 calculation, see Table S8. The first three spin-free states (δ_E) correspond to the splitting under C_2 symmetry of the complex, while the first six SOC energy levels (Δ_E) are the final splitting in six KDs.

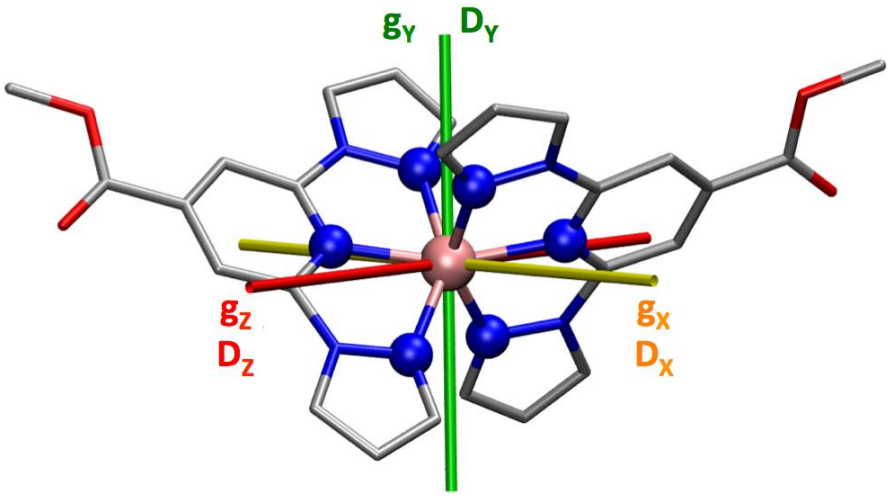

Figure S12. Orientation of the computed $\bar{\boldsymbol{g}}$ and $\bar{\boldsymbol{D}}$ matrices for **1** obtained with the ORCA/NEVPT2 calculation (the orientations with other calculations are practically coincident).

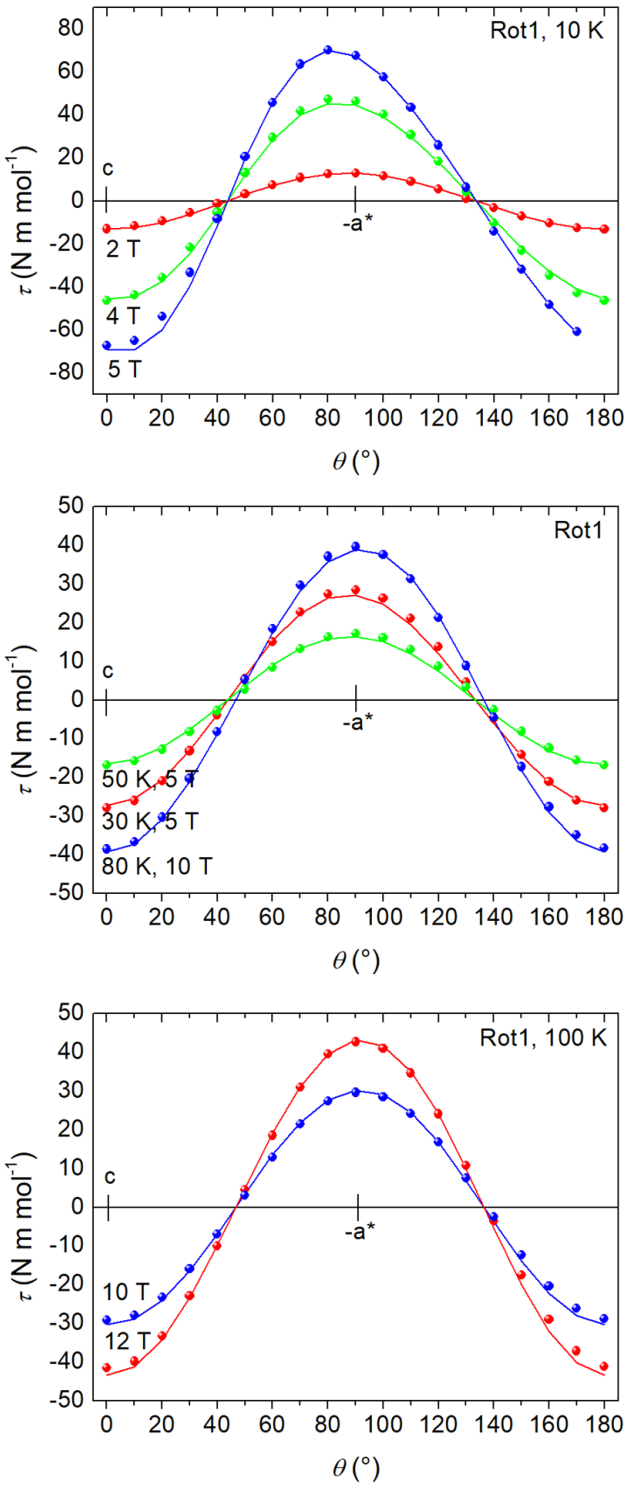

Figure S13. Experimental (dots) and MOLCAS-computed (lines, N m mol^{-1}) torque values for Rot1 at different temperatures and fields.

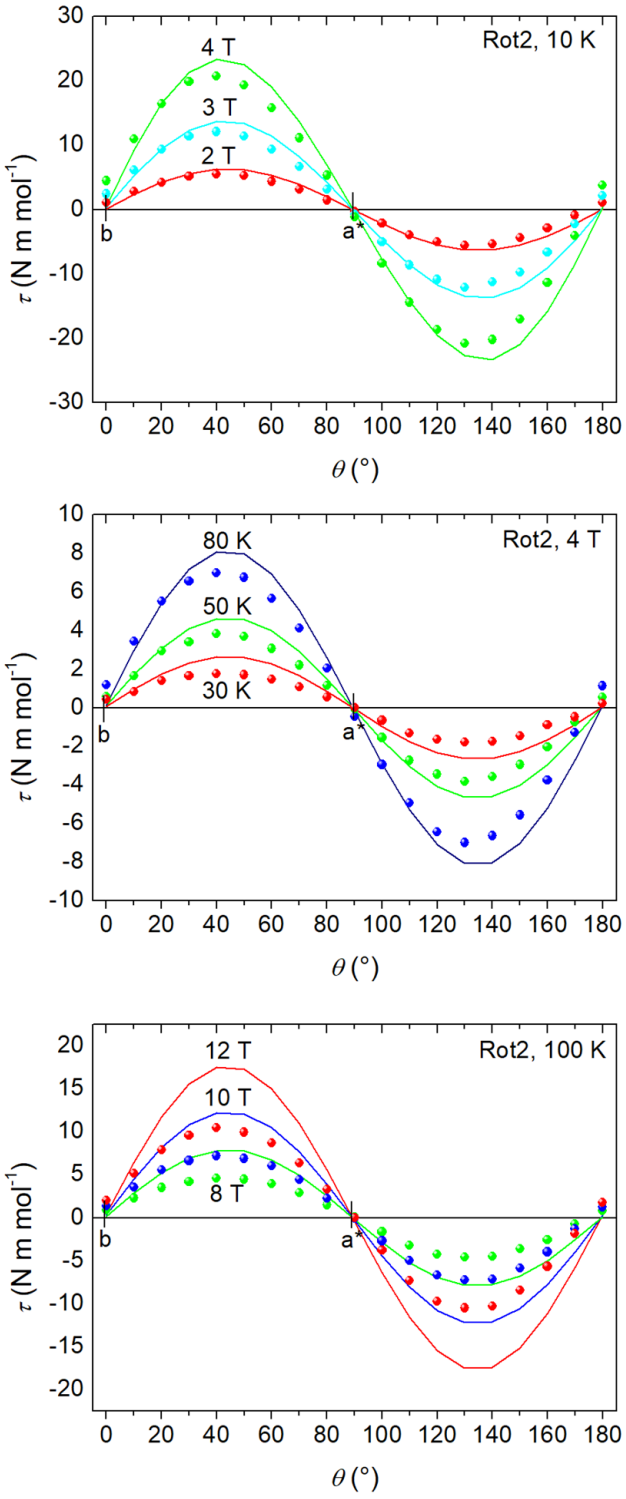

Figure S14. Experimental (dots) and MOLCAS-computed (lines, N m mol^{-1}) torque values for Rot2 at different temperatures and fields.

References

[S1] Bruker *SAINT*. Bruker AXS Inc., Madison, Wisconsin, USA, **2012**.

[S2] G. M. Sheldrick, *SADABS*. University of Göttingen, Germany, **1996**.

[S3] a) G. M. Sheldrick, *Acta Crystallogr. Sect. A* **2008**, *64*, 112–122; b) G. M. Sheldrick, *Acta Crystallogr. Sect. C* **2015**, *71*, 3–8.

[S4] C. F. Macrae, I. J. Bruno, J. A. Chisholm, P. R. Edgington, P. McCabe, E. Pidcock, L. Rodriguez-Monge, R. Taylor, J. van de Streek, P. A. Wood, *J. Appl. Crystallogr.* **2008**, *41*, 466– 470.

[S5] G. A. Bain, J. F. Berry, *J. Chem. Educ.* **2008**, *85*, 532−536.

[S6] a) K. S. Cole, R.H. Cole, *J. Chem. Phys.* **1941**, *9*, 341–352; b) C. Dekker, A. F. M. Arts, H. W. Wijn, A. J. van Duyneveldt, J. A. Mydosh, *Phys Rev. B* **1989**, *40*, 11243–11251.

[S7] a) G. Karlström, R. Lindh, P.-Å. Malmqvist, B. O. Roos, U. Ryde, V. Veryazov, P.-O. Widmark, M. Cossi, B. Schimmelpfennig, P. Neograd y, L. Seijo, *Comput. Mater. Sci.* **2003**, *28*, 222–239; b) V. Veryazov, P.-O. Widmark, L. Serrano-Andrés, R. Lindh, B. O. Roos, *Int. J. Quantum Chem.* **2004**, *100*, 626–635; c) F. Aquilante, L. De Vico, N. Ferré, G. Ghigo, P.- Å. Malmqvist, P. Neogrády, T. B. Pedersen, M. Pitoňák, M. Reiher, B. O. Roos, L. Serrano-Andrés, M. Urban, V. Veryazov, R. Lindh, *J. Comput. Chem.* **2010**, *31*, 224–247.

[S8] F. Neese, *WIREs Comput. Mol. Sci* **2012**, *2*, 73–78.

[S9] L. F. Chibotaru, L. Ungur, C. Aronica, H. Elmoll, G. Pillet, D. Luneau, *J. Am. Chem. Soc.* **2008**, *130*, 12445–12455.

[S10] L. F. Chibotaru, L. Ungur, A. Soncini, *Angew. Chem. Int. Ed.* **2008**, *47*, 4126–4129.

[S11] B. O. Roos, V. Veryazov, P.-O. Widmark, *Theor. Chim. Acta* **2004**, *111*, 345–351.

[S12] B. O. Roos, R. Lindh, P.-Å. Malmqvist, V. Veryazov, P.-O. Widmark, *J. Phys. Chem. A* **2004**, *108*, 2851–2858.

[S13] B. O. Roos, R. Lindh, P.-Å. Malmqvist, V. Veryazov, P.-O. Widmark, *J. Phys. Chem. A* **2005**, *109*, 6575–6579.

[S14] B. O. Roos, R. Lindh, P.-Å. Malmqvist, V. Veryazov, P.-O. Widmark, *Chem. Phys. Lett.* **2005**, *409*, 295–299.

[S15] C. Angeli, R. Cimiraglia, S. Evangelisti, T. Leininger, J.-P. Malrieu, *J. Chem. Phys.* **2001**, *114*, 10252–10264.

[S16] C. Angeli, R. Cimiraglia, J.-P. Malrieu, *Chem. Phys. Lett.* **2001**, *350*, 297–305.

[S17] C. Angeli, R. Cimiraglia, J.-P. Malrieu, *J. Chem. Phys.* **2002**, *117*, 9138–9153.

[S18] F. Weigend, R. Ahlrichs, *Phys. Chem. Chem. Phys.* **2005**, *7*, 3297–3305.

[S19] F. Weigend, *Phys. Chem. Chem. Phys.* **2006**, *8*, 1057–1065.

[S20] S. Stoll, A. Schweiger, *J. Magn. Reson.* **2006**, *178*, 42–55.